

Geometrical structure and thermal conductivity of dust aggregates formed via ballistic cluster-cluster aggregation

Sota Arakawa, Masaki Takemoto, and Taishi Nakamoto

Department of Earth and Planetary Sciences, Tokyo Institute of Technology, 2-12-1 Ookayama, Meguro, Tokyo, 152-8551, Japan.

**E-mail: arakawa.s.ac@m.titech.ac.jp*

.....
We herein report a theoretical study of the geometrical structure of porous dust aggregates formed via ballistic cluster-cluster aggregation (BCCA). We calculated the gyration radius R_{gyr} and the graph-based geodesic radius R_{geo} as a function of the number of constituent particles N . We found that $R_{\text{gyr}}/r_0 \sim N^{0.531 \pm 0.011}$ and $R_{\text{geo}}/r_0 \sim N^{0.710 \pm 0.013}$, where r_0 is the radius of constituent particles. Furthermore, we defined two constants that characterize the geometrical structure of fractal aggregates: D_f and α . The definition of D_f and α are $N \sim (R_{\text{gyr}}/r_0)^{D_f}$ and $R_{\text{geo}}/r_0 \sim (R_{\text{gyr}}/r_0)^\alpha$, respectively. Our study revealed that $D_f \simeq 1.88$ and $\alpha \simeq 1.34$ for the clusters of the BCCA.

In addition, we also studied the filling factor dependence of thermal conductivity of statically compressed fractal aggregates. From this study, we reveal that the thermal conductivity of statically compressed aggregates k is given by $k \sim 2k_{\text{mat}}(r_c/r_0)\phi^{(1+\alpha)/(3-D_f)}$, where k_{mat} is the material thermal conductivity, r_c is the contact radius of constituent particles, and ϕ is the filling factor of dust aggregates.

.....
Subject Index E21, I04, I10, J44

1. Introduction

The study of the aggregation of small dust particles into larger aggregates is crucial for understanding the fundamental processes in astrophysics and geophysics. For example, the growth of aerosol or haze particles in the atmosphere causes the scattering and absorption of the sunlight [e.g., 1]. In addition to this, the aggregation of dust particles also occurs in the mineral clouds of exoplanets and hence understanding the fundamental processes involved in the formation process of dust aggregates in exoplanets is imperative to interpret the transmission spectra [e.g., 2, 3]. In addition, the aggregation of dust particles in the solar nebula is the first step towards the formation of the planets [e.g., 4–7], and the density evolution of dust aggregates is considered to be the key to understanding the evolution from nm- or μm -sized dust grains to km-sized small bodies [e.g., 8–11]. The resulting aggregates frequently have a complex and fractal structure with an extremely low filling factor [e.g., 12–14]. Therefore, understanding the geometrical structure of these fractal aggregates and its influence on the physical properties such as the thermal conductivity and the compressive strength is of immense current interest.

For porous dust aggregates composed of micron-sized SiO₂ glass grains, the thermal conductivity is obtained by several experimental studies [e.g., 15, 16], and it is empirically known that the thermal conductivity is approximately proportional to the square of the filling factor [17–19]. However, the theoretical explanation of the dependence of thermal conductivity on the filling factor is still lacking.

In contrast to the thermal conductivity, the filling factor dependence of the tensile strength of porous dust aggregates is well understood [20]. The tensile strength of porous dust aggregates is evaluated from the fractal structure of dust aggregates and the maximum force required to separate two sticking particles. The compression strength would also be evaluated from the fractal structure of dust aggregates and the rolling energy needed to rotate a constituent particle around its connecting points [21].

In this paper, we describe the geometrical structure of porous dust aggregates formed in astrophysical environments. We present the calculation of the gyration radius (which is defined in Section 2.1) and the graph-based geodesic radius (which is defined in Section 2.2) of porous dust aggregates. Subsequently, we present the interpretations of the filling factor dependence of thermal conductivity from the geometrical structure, and we also confirm the validity of our theoretical understanding by comparing it with the result of direct numerical calculations in Section 3. Finally, we also present the modified interpretation of the filling factor dependence of compression strength and the average coordination number of dust aggregates in Section 4.

2. Ballistic cluster-cluster aggregation

In the early stage of dust growth in astrophysical environments such as protoplanetary disks and circumplanetary disks, the collision velocity is sufficiently low to avoid collisional compaction and collisions between similar-sized dust aggregates are dominant [e.g., 22, 23]. Therefore, the shape of dust aggregates in astrophysical environments is expected to resemble the clusters of ballistic cluster-cluster aggregation (BCCA). The BCCA clusters are formed by the sticking of two equal sized BCCA clusters with no restructuring (see Figure 3(a) of Okuzumi et al. [24]). We prepare BCCA clusters in the following procedure: (1) prepare an aggregate composed of 2^i particles (initially $i = 0$), (2) copy this aggregate and change the orientation of the copy randomly, (3) by ballistic sticking of these two aggregates with a randomly chosen offset, make a new aggregate composed of 2^{i+1} particles, (4) continue the procedure (1)–(3). As shown in Figure 1, a BCCA cluster has a highly porous structure. In this study, we assumed that all constituent particles (hereinafter referred to as “monomers”) are spherical and have the same radius r_0 .

2.1. Gyration radius

For the quantitative analysis of the structure of porous aggregates, we need to define a typical cluster radius. Here, we use the gyration radius R_{gyr} , which is customary in aggregation studies [e.g., 23–25] defined by

$$R_{\text{gyr}} \equiv \left(\frac{1}{2N^2} \sum_i^N \sum_j^N (\mathbf{x}_i - \mathbf{x}_j)^2 \right)^{1/2} \equiv \left(\frac{1}{N} \sum_i^N (\mathbf{x}_i - \mathbf{x}_o)^2 \right)^{1/2}, \quad (1)$$

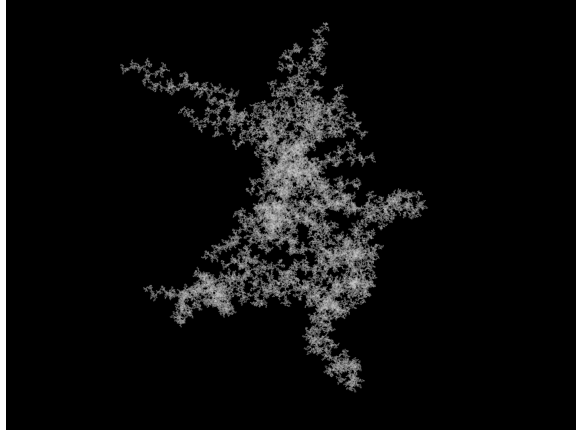


Fig. 1 Projection of a three-dimensional dust aggregate formed via ballistic cluster-cluster aggregation (BCCA). The number of constituent particles is $N = 2^{16} = 65536$.

where N is the number of constituent monomers, \mathbf{x}_i is the coordinate of the i -th monomer, and \mathbf{x}_o is the coordinate of the center of mass.

We carried out 20 growth sequences of N -body simulations of BCCA as previous studies [24, 25]. Here we show the geometric mean of the gyration radius R_{gyr} as the function of the number of monomers N in Figure 2(a). We found that the gyration radius R_{gyr} is given by

$$\log_{10} \frac{R_{\text{gyr}}}{r_0} = (0.531 \pm 0.011) \log_{10} N + (-0.012 \pm 0.006), \quad (2)$$

and given uncertainties are the standard errors. The structure of BCCA clusters is therefore described in terms of the fractal dimension D_f , which is defined as

$$N \sim \left(\frac{R_{\text{gyr}}}{r_0} \right)^{D_f}. \quad (3)$$

Our numerical data shows that D_f is

$$D_f \simeq \frac{1}{0.531} \simeq 1.88, \quad (4)$$

or $1.85 < D_f < 1.92$ when we take uncertainty into consideration. This result is consistent with previous studies [24–26].

The effective volume of BCCA clusters V is evaluated as $V \sim 4\pi R_{\text{gyr}}^3/3$ and the volume of monomers is $V_0 = 4\pi r_0^3/3$. The filling factor of BCCA clusters ϕ is given by

$$\phi = \frac{NV_0}{V} \sim \frac{N}{(R_{\text{gyr}}/r_0)^3} \sim N^{1-3/D_f}. \quad (5)$$

Therefore, we can calculate the filling factor of BCCA clusters from the number of monomers.

2.2. Graph-based geodesic radius

Granular materials and dust aggregates transmit compressive stresses via a network of force chains [e.g., 27]. Further, the chains of monomers also conduct heat [e.g., 28]. Therefore, understanding the chain structure within dust aggregates is essential, especially for the study of the mechanical and heat transfer properties. Here, we introduce *the graph geodesic* and *the*

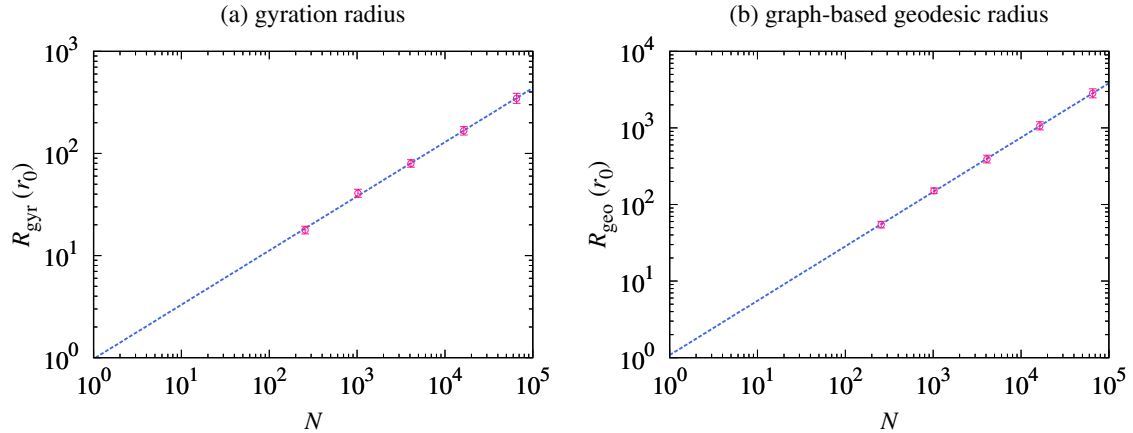


Fig. 2 (a) Fitting of the gyration radius of BCCA clusters R_{gyr} as a function of the number of monomers N . (b) Fitting of the graph-based geodesic radius of BCCA clusters R_{geo} as a function of N . The circles represent the averaged data with vertical error bars of twice the standard error. The dashed line is the best-fit obtained from the weighted least-squares method.

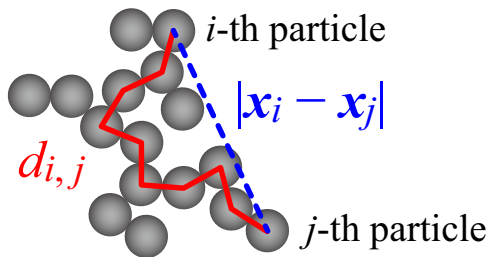


Fig. 3 Schematic description of the distance between i -th and j -th particles, $|\mathbf{x}_i - \mathbf{x}_j|$, and the graph geodesic between i -th and j -th particles, $d_{i,j}$. It is clear that the graph geodesic $d_{i,j}$ is larger than the distance $|\mathbf{x}_i - \mathbf{x}_j|$.

graph-based geodesic radius. Figure 3 schematically illustrates a BCCA cluster. The distance between i -th and j -th particles is $|\mathbf{x}_i - \mathbf{x}_j|$, and we define the graph geodesic between i -th and j -th particles as $d_{i,j}$ in Figure 3. Considering the graph structure of BCCA cluster, which is a tree (i.e., a connected acyclic graph), we can uniquely determine the graph geodesic $d_{i,j}$.

The typical length of the chain of monomers is obtained using the same method as the definition of R_{gyr} . We define the graph-based geodesic radius R_{geo} as

$$R_{\text{geo}} \equiv \left(\frac{1}{2N^2} \sum_i \sum_j d_{i,j}^2 \right)^{1/2}. \quad (6)$$

It is clear that $d_{i,j}^2 \geq (\mathbf{x}_i - \mathbf{x}_j)^2$ and then $R_{\text{geo}} \geq R_{\text{gyr}}$ by definition. Here we show the geometric mean of the graph-based geodesic radius R_{geo} as a function of the number of monomers N over 20 runs in Figure 2(b). We found that the graph-based geodesic radius

R_{geo} is given by

$$\log_{10} \frac{R_{\text{geo}}}{r_0} = (0.710 \pm 0.013) \log_{10} N + (0.034 \pm 0.007), \quad (7)$$

and given uncertainties are the standard errors.

Here, we consider the ratio of R_{geo} and R_{gyr} . The ratio of R_{geo} and R_{gyr} is given by

$$\frac{R_{\text{geo}}}{r_0} \sim \left(\frac{R_{\text{gyr}}}{r_0} \right)^\alpha, \quad (8)$$

where α is the dimensionless constant and the constant α must depend on the aggregation process of clusters. For BCCA clusters, we found that

$$\alpha \simeq \frac{0.710}{0.531} \simeq 1.34, \quad (9)$$

or $1.29 < \alpha < 1.39$ when we take uncertainty into consideration.

2.3. Bifractality of statically compressed BCCA clusters

In the early stage of dust growth, the fractal dimension of dust aggregates is $D_f \simeq 1.9$. When the dust aggregates grow into cm-sized cluster, BCCA clusters are dynamically compressed by dust-dust collisions [e.g., 29] and/or statically compressed by ram pressure of the disk gas [e.g., 30]. Although it depends on the physical properties of the disk and the monomers, the compression mechanism for icy aggregates composed of submicron-size monomers in the minimum mass solar nebula [31, 32] is the static compression by ram pressure [30]. In this study, we focus on the geometrical structure of statically compressed BCCA clusters.

The geometrical structure of statically compressed BCCA clusters is characterized by bifractality [21]. Kataoka et al. [21] calculated the average number of particles in spheres of radii r_{in} , N_{in} . For statically compressed BCCA clusters, N_{in} is approximately given by

$$N_{\text{in}} \sim \left(\frac{r_{\text{in}}}{r_0} \right)^{D_f} \quad (r_{\text{in}} \ll r_{\text{tr}}), \quad (10)$$

$$N_{\text{in}} \sim \phi \left(\frac{r_{\text{in}}}{r_0} \right)^3 \quad (r_{\text{in}} \gg r_{\text{tr}}), \quad (11)$$

and the transition radius r_{tr} is evaluated as $r_{\text{tr}} \sim \phi^{1/(D_f-3)} r_0$. In other words, the fractal dimension becomes three on a large scale, while it remains 1.9, i.e., D_f of BCCA, on a small scale. This structure evolution suggests that the static compression reconstructs the fractal aggregate first on a large scale, because of the weak compressive strength on a large scale [21]. Therefore, we can imagine that it is possible to understand the physical properties of statically compressed BCCA clusters from the geometrical structure of small BCCA clusters preserved in compressed aggregates (hereinafter referred to as ‘‘BCCA cells’’). Figure 4 shows the schematic description of a BCCA cell in the compressed BCCA cluster.

It is important to note that the geometrical structure of dynamically compressed BCCA clusters is also characterized by bifractality [e.g., 6]. The resulting fractal dimension is approximately 2.5 on a large scale and it remains D_f of BCCA on a small scale. Therefore, bifractality is a common characteristic of compressed BCCA clusters. We also hypothesize that this bifractality is a common structure for compressed fractal aggregates although the initial cluster is not originated from BCCA but other aggregation processes, for example, diffusion-limited cluster aggregation [e.g., 33] or reaction-limited cluster aggregation [e.g., 34]. We will, however, need to confirm this hypothesis in the future.

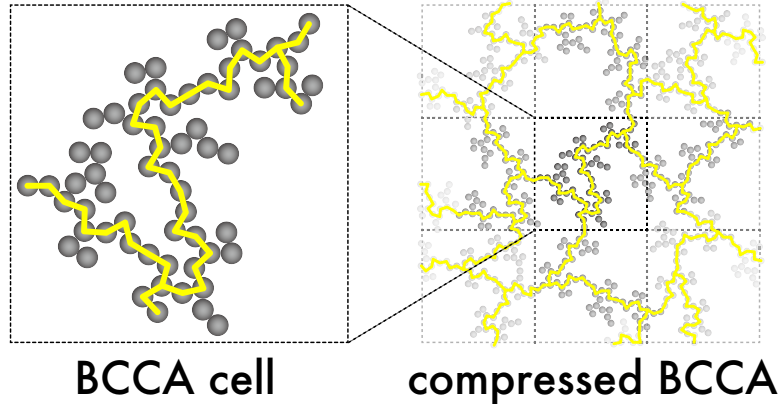


Fig. 4 Schematic description of a BCCA cell in the compressed BCCA cluster. The yellow lines represent the possible heat paths.

3. Thermal conductivity

In this section, we calculate the thermal conductivity of compressed BCCA clusters and demonstrate the manner in which the geometrical structure affects the thermal conductivity.

3.1. Methods

We calculate the thermal conductivity of compressed BCCA clusters composed of $16384 (= 2^{14})$ monomers. The snapshots used in this study and used in our previous study (Arakawa et al. [19]) are the same and were prepared by Tatsuuma et al. [20]. The methods of the thermal conductivity calculation are described in our previous studies [18, 19], which we briefly summarize it here.

Dust aggregates are statically compressed in a cubic periodic boundary (see Figure 1 of Arakawa et al. [18]). We consider one-directional heat flow from the lower to the upper boundary plane. The thermal conductivity of a dust aggregate in a cubic periodic boundary k is given by

$$k = 2k_{\text{mat}} \frac{r_c}{r_0} f, \quad (12)$$

where f is a dimensionless function of ϕ , k_{mat} is the material thermal conductivity, and r_c is the contact radius of monomer grains. The normalized thermal conductivity f is given by

$$f \equiv \frac{r_0 L}{S} \sum_{\text{upper}} \frac{T_j - T_i}{\Delta T}, \quad (13)$$

where L is the length of the side of the cube, $S = L^2$ is the area of the upper and lower boundaries, T_i is the temperature of i -th monomer, and ΔT is the temperature difference between the upper and lower boundaries. We took the sum of contacts between the i -th grain on the upper boundary and j -th grain inside the boundaries (see Arakawa et al. [18] for details).

In this study, we also consider the series connection of dust aggregates in a cubic periodic boundary (see Figure 5). It is expected that the series connection of dust aggregates would reduce the artificial effects of the boundary condition on the thermal conductivity calculations.

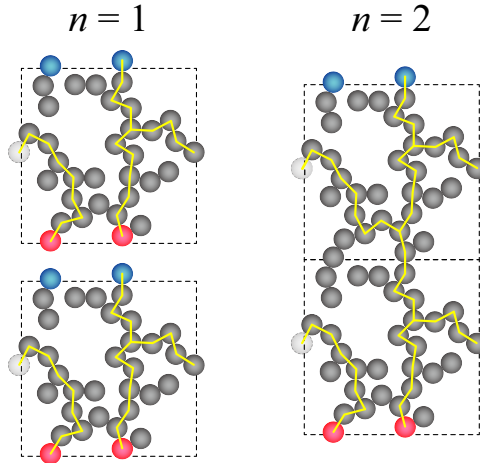


Fig. 5 Schematic description of the series connection of dust aggregates in a cubic periodic boundary. The blue monomers are on the upper boundary and the reds are on the lower boundary, and the yellow lines represent the heat paths. The series connection of dust aggregates would reduce the artificial effects of the boundary condition.

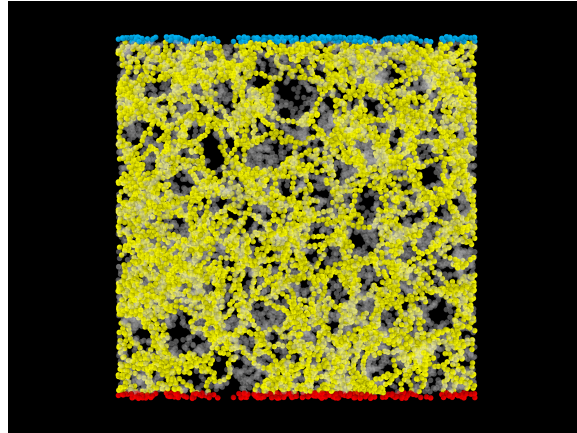


Fig. 6 An example snapshot of a compressed BCCA cluster in a cubic periodic boundary. The blue monomers are on the upper boundary and the reds are on the lower boundary. The yellow monomers represent the heat paths and the grays are the non-contributing monomers. The filling factor of the aggregates is $\phi = 10^{-1.5}$.

3.2. Filling factor dependence

Figure 6 shows the projection of three-dimensional compressed BCCA cluster in a cubic periodic boundary. The blue monomers are on the upper boundary and the reds are on the lower boundary. The yellow monomers represent the heat paths and the grays are the non-contributing monomers. The filling factor of the aggregates is $\phi = 10^{-1.5}$. It is clear that not all monomers contribute to the heat transfer within the dust aggregate.

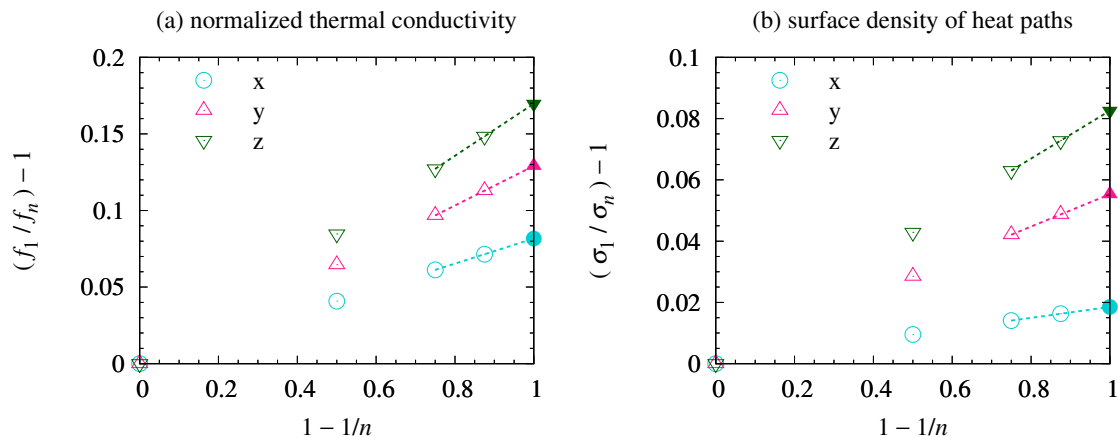


Fig. 7 (a) Example calculation of f_∞ (filled marker) using $f_1, f_2, f_4,$ and f_8 (open markers). (b) Example calculation of σ_∞ (filled marker) by using $\sigma_1, \sigma_2, \sigma_4,$ and σ_8 (open markers). The aggregate used in this calculation is the same that used in Figure 6. We calculated f_∞ and σ_∞ from three directions ($x, y,$ and z).

It is predicted that the normalized thermal conductivity of dust aggregates in a series connection of n cubes, f_n , is given by

$$\frac{1}{f_n} \simeq \frac{1}{n} \left(\frac{1}{f_1} + \frac{n-1}{f_\infty} \right), \quad (14)$$

where f_∞ is defined as

$$f_\infty = \lim_{n \rightarrow \infty} f_n. \quad (15)$$

We can rewrite Equation (14) as

$$\frac{f_1}{f_n} - 1 \simeq \left(\frac{f_1}{f_\infty} - 1 \right) \left(1 - \frac{1}{n} \right), \quad (16)$$

and we found that $(f_1/f_n) - 1$ is approximately proportional to $1 - (1/n)$. In Figure 7(a), we confirmed that the relation between $(f_1/f_n) - 1$ and $1 - (1/n)$ works well. Therefore, we can evaluate f_∞ using f_4 and f_8 as follows:

$$f_\infty \simeq \left(\frac{2}{f_8} - \frac{1}{f_4} \right)^{-1}. \quad (17)$$

Figure 8(a) shows the normalized thermal conductivity for the limiting case of $n \rightarrow \infty$, f_∞ , as a function of the filling factor ϕ . We used 10 snapshot data for each ϕ obtained from different compression simulations [20] and calculated f_∞ from three directions. The circles represent the geometric mean of 30 calculation results of the temperature structure, with vertical error bars of twice the standard error. We found that f_∞ is given by

$$\log_{10} f_\infty = (2.068 \pm 0.034) \log_{10} \phi + (-0.022 \pm 0.007), \quad (18)$$

and given uncertainties are the standard errors. This result is consistent with those of previous studies [18, 19].

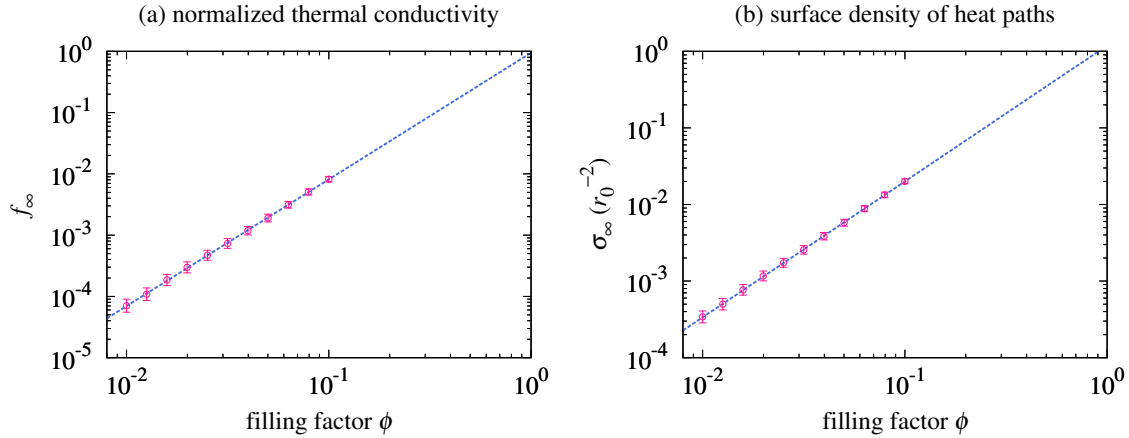


Fig. 8 (a) Fitting of the normalized thermal conductivity for the limiting case of $n \rightarrow \infty$, f_∞ , as a function of the filling factor ϕ . (b) Fitting of the surface density of heat paths for the limiting case of $n \rightarrow \infty$, σ_∞ , as a function of ϕ . The circles represent the averaged data with vertical error bars of twice the standard error. The dashed line is the best-fit obtained from the weighted least-squares method.

3.3. Surface density of heat paths

The thermal conductivity of dust aggregates must be affected by the typical length of the chain of monomers R_{geo} and the surface density of heat paths σ . Here, we introduce the number of heat paths at the temperature T , $\mathcal{N}_{\text{path}}(T)$. We define $\mathcal{N}_{\text{path}}(T)$ as the number of contacts between two monomers whose temperatures are T_i and T_j with $T_i < T < T_j$. Thereafter, the average number of heat paths $\overline{\mathcal{N}_{\text{path}}}$ is given by

$$\overline{\mathcal{N}_{\text{path}}} \equiv \frac{1}{\Delta T} \int_{-\Delta T/2}^{+\Delta T/2} dT \mathcal{N}_{\text{path}}(T), \quad (19)$$

where the temperature at the upper and lower boundaries are $-\Delta T/2$ and $+\Delta T/2$, respectively. The surface density of heat paths σ is given by

$$\sigma \equiv \frac{\overline{\mathcal{N}_{\text{path}}}}{S}. \quad (20)$$

The average number of heat paths $\overline{\mathcal{N}_{\text{path}}}$ depends on the number of connected cubes, n . In Figure 5, $\overline{\mathcal{N}_{\text{path}}} = 3/2$ for the case of $n = 1$ and $\overline{\mathcal{N}_{\text{path}}} = 409/281$ for the case of $n = 2$. As well as f_∞ , we evaluated the surface density of heat paths for the limiting case of $n \rightarrow \infty$, σ_∞ . In Figure 7(b), we confirmed that σ_∞ can be predicted as follows:

$$\sigma_\infty \simeq \left(\frac{2}{\sigma_8} - \frac{1}{\sigma_4} \right)^{-1}, \quad (21)$$

where σ_n is the surface density of heat paths within a dust aggregate in a series connection of n cubes. Figure 8(b) shows the surface density of heat paths for the limiting case of $n \rightarrow \infty$, σ_∞ , as a function of the filling factor ϕ . We found that

$$\log_{10} \frac{\sigma_\infty}{r_0^{-2}} = (1.775 \pm 0.025) \log_{10} \phi + (0.076 \pm 0.005), \quad (22)$$

and given uncertainties are the standard errors.

For a BCCA cell, we can imagine that the average number of heat paths is

$$\overline{\mathcal{N}_{\text{path}}} \sim \mathcal{O}(1). \quad (23)$$

Thereafter, the surface density of heat paths within a BCCA cell is given by

$$\sigma = \frac{\overline{\mathcal{N}_{\text{path}}}}{S} \sim R_{\text{gyr}}^{-2}. \quad (24)$$

The relation between the gyration radius R_{gyr} and the filling factor ϕ is

$$\frac{R_{\text{gyr}}}{r_0} \sim N^{1/D_f} \sim \phi^{1/(D_f-3)}, \quad (25)$$

and we obtain the relation between σ and ϕ :

$$\sigma \sim \phi^{2/(3-D_f)} r_0^{-2}. \quad (26)$$

We found that $1.85 < D_f < 1.92$ in Section 2.1, therefore, we obtain $1.74 < 2/(3 - D_f) < 1.85$. The range of $2/(3 - D_f)$ matches the numerical result, $\sigma \sim \phi^{1.775 \pm 0.025} r_0^{-2}$. This fact validates the assumption that $\overline{\mathcal{N}_{\text{path}}} \sim \mathcal{O}(1)$ for BCCA cells.

We note that the tensile strength of compressed BCCA clusters, P_t , is approximately given by $P_t \sim \sigma F_c$, where $F_c = 3\pi\gamma r_0/2$ is the maximum force required to separate two sticking monomers and γ is the surface energy [5]. Therefore, the tensile strength is given by

$$P_t \sim \gamma r_0^{-1} \phi^{1.775 \pm 0.025}, \quad (27)$$

which is consistent with the numerical result of Tatsuuma et al. [20], $P_t \simeq 0.6\gamma r_0^{-1} \phi^{1.8}$. The coincidence of the filling factor dependence may indicate not only the number of heat paths but the number of force chains is also on the order of unity for BCCA cells.

3.4. Understanding the filling factor dependence of the thermal conductivity

Here, we demonstrate the manner in which the filling factor dependence of the thermal conductivity is derived from the geometrical structure. For compressed BCCA clusters, the fractal dimension is three on a large scale, then the thermal conductivity of compressed BCCA clusters should be the same as the thermal conductivity of BCCA cells.

The spatial scale of BCCA cells is $L \sim R_{\text{gyr}}$ and the area of the BCCA cells is $S \sim R_{\text{gyr}}^2$, where $R_{\text{gyr}} \sim N^{1/D_f} r_0$ is the gyration radius of a BCCA cell and N is the number of monomers in a BCCA cell. The surface density of heat paths is approximately given by $\sigma \sim R_{\text{gyr}}^{-2}$. The typical temperature difference between two contacting monomers, δT , is also given by

$$\delta T \sim \frac{\Delta T}{R_{\text{geo}}/r_0}, \quad (28)$$

where ΔT is the temperature difference between the upper and lower region of a BCCA cell. The heat conductance at the contact of two monomers, H , is [e.g., 35, 36]

$$H = 2k_{\text{mat}} r_c, \quad (29)$$

and the heat flow at the contact of two monomers, I , is $I \sim H\delta T$. Therefore, the heat flow density within the BCCA cell is

$$k \frac{\Delta T}{L} \sim \sigma H \delta T, \quad (30)$$

and the thermal conductivity k is rewritten as follows:

$$k \sim 2k_{\text{mat}} \frac{r_c}{r_0} \frac{r_0^2}{R_{\text{gyr}} R_{\text{geo}}}. \quad (31)$$

The normalized thermal conductivity f of the BCCA cell (and the compressed BCCA cluster) is therefore given by

$$f \sim \frac{r_0^2}{R_{\text{gyr}} R_{\text{geo}}} \sim N^{-(1+\alpha)/D_f}. \quad (32)$$

The relation between N and ϕ is $N \sim \phi^{D_f/(D_f-3)}$, then we obtain the following equation:

$$f \sim \phi^{(1+\alpha)/(3-D_f)} \sim \phi^{2.09}. \quad (33)$$

The derived relation shows excellent coincidence with our numerical result, $f \sim \phi^{2.068 \pm 0.034}$.

4. Discussion

4.1. Reinterpretation of the filling factor dependence of the compressive strength

We can also derive the filling factor dependence of the compressive strength of compressed BCCA clusters from the geometrical structure. In this section, we evaluate the compressive strength P_c as Kataoka et al. [21] did.

The compressive force on the surface area of the BCCA cell F_c and the compressive strength P_c are given by

$$F_c \sim P_c R_{\text{gyr}}^2. \quad (34)$$

The length of the force chain within the BCCA cell is R_{geo} . Since the compression is accompanied by the rolling of pairs of monomers in the force chain, the work required for compression can be given by

$$F_c R_{\text{geo}} \sim E_{\text{roll}}, \quad (35)$$

where $E_{\text{roll}} = 6\pi^2 \gamma r_0 \xi_{\text{cr}}$ is the energy needed to rotate a monomer around its connection point by $\pi/2$ rad called the rolling energy, and ξ_{cr} is the critical rolling displacement [5]. Subsequently, we found that the compressive strength P_c is given by

$$P_c \sim \frac{E_{\text{roll}}}{R_{\text{gyr}}^2 R_{\text{geo}}} \sim \frac{E_{\text{roll}}}{r_0^3} \phi^{(2+\alpha)/(3-D_f)}, \quad (36)$$

and $(2+\alpha)/(3-D_f) \simeq 2.99$ for compressed BCCA clusters. The derived relation shows an excellent agreement with the numerical results of Kataoka et al. [21], i.e., $P_c \sim (E_{\text{roll}}/r_0^3) \phi^3$.

We note that the original explanation by Kataoka et al. [21] might not be accurate. Kataoka et al. [21] evaluated the work required for compression as

$$F_c R_{\text{gyr}} \sim E_{\text{roll}}, \quad (37)$$

and the filling factor dependence of the compressive strength was obtained as

$$P_c \sim \frac{E_{\text{roll}}}{R_{\text{gyr}}^3} \sim \frac{E_{\text{roll}}}{r_0^3} \phi^{3/(3-D_f)}. \quad (38)$$

This estimate was based on the assumption that the compression is accompanied by the rolling of single pair of monomers in a BCCA cell. In this derivation, $3/(3-D_f) \simeq 2.69$ and it might not reproduce their numerical results. Although our findings suggest that the α parameter associated with the chain length plays a significant role on the compression of dust aggregates, further studies on the force distribution within compressed fractal aggregates are required.

4.2. Revisiting the average coordination number of compressed aggregates

The average coordination number (i.e., the average number of contacts per monomer) Z increases as an aggregate is compressed. Arakawa et al. [19] found that, for compressed BCCA clusters, the filling factor dependence of Z is given by $Z = 2 + 9.38\phi^{1.62}$. Here, we derive this equation from the geometrical structure.

Considering the graph structure of BCCA cluster, which is a tree (i.e., a connected acyclic graph), the average coordination number of a compressed BCCA clusters is

$$Z \sim \frac{2N + C}{N}, \quad (39)$$

where the constant C is the number of the inter-cell contacts per BCCA cell. The number of the faces, edges, and corners within a cube is 6, 12, and 8, respectively. Subsequently, we assume that the number of the inter-cell contacts per BCCA cell is $C \sim 9$.

We define the deviation of the coordination number from two, $\zeta \equiv Z - 2$. The deviation ζ is given by

$$\zeta \sim \frac{C}{N} \sim C\phi^{D_f/(3-D_f)}, \quad (40)$$

and $1.60 < D_f/(3 - D_f) < 1.79$ when we take the uncertainty of D_f into consideration. Therefore, we obtain the following equation:

$$Z = 2 + C\phi^{D_f/(3-D_f)}, \quad (41)$$

which is consistent with the numerical result of Arakawa et al. [19], although the uncertainty of $D_f/(3 - D_f)$ is large and future studies on both the fractal dimension analysis and the average coordination number are essential. We note that the fractal dimension D_f depends on the formation process of dust aggregates. Thereofre, the average coordination number Z also depends on the formation process of dust aggregates, as reported in Seizinger and Kley [37].

The compressive strength P_c is also affected by the average coordination number Z . If the average coordination number is $Z \simeq 2$, nearly all the monomers can roll when they are compressed. Therefore, the interparticle force is close to the rolling friction force and the compressive strength is given by Equation (36). On the other hand, in the high-density region ($\phi \gg 0.1$ and $Z \gg 2$), most of the particles cannot roll freely and the compressive strength is larger than the evaluated value for the case of $Z \simeq 2$ [e.g., 38–41]. Then, we expect that the compressive strength would be given by the sliding friction force in the high-density limit [40], although future studies are required to understand this in detail.

5. Summary

In this study, we conducted the numerical simulations of the BCCA of small dust particles and calculated the geometrical structure of the fractal dust aggregates. Additionally, we derived the filling factor dependence of the physical properties of porous dust aggregates. Our key findings are summarized as follows.

- (1) We calculated the gyration radius R_{gyr} and the graph-based geodesic radius R_{geo} as the functions of the number of constituent particles N . We found that $R_{\text{gyr}}/r_0 \sim N^{0.531 \pm 0.011}$ and $R_{\text{geo}}/r_0 \sim N^{0.710 \pm 0.013}$, where r_0 is the radius of constituent particles. Thereafter, we defined two constants which characterize the geometrical structure

of fractal aggregates: D_f and α . The definition of D_f and α are $N \sim (R_{\text{gyr}}/r_0)^{D_f}$ and $R_{\text{geo}}/r_0 \sim (R_{\text{gyr}}/r_0)^\alpha$, respectively. We revealed that $D_f \simeq 1.88$ and $\alpha \simeq 1.34$ for BCCA clusters.

- (2) Kataoka et al. [21] found that the geometrical structure of statically compressed BCCA clusters is characterized by bifractality. This structure evolution suggests that the static compression reconstructs the fractal aggregate first on a large scale because of the weak compressive strength on a large scale. Therefore, we can imagine that it is possible to understand the physical properties of statically compressed BCCA clusters from the geometrical structure of small BCCA clusters preserved in compressed aggregates (“BCCA cells”).
- (3) We investigated the filling factor dependence of thermal conductivity of statically compressed aggregates. We found that the filling factor dependence can be interpreted from the geometrical structure of dust aggregates. The thermal conductivity of statically compressed aggregates k is given by $k \sim 2k_{\text{mat}}(r_c/r_0)\phi^{(1+\alpha)/(3-D_f)}$, where k_{mat} is the material thermal conductivity, r_c is the contact radius of constituent particles, and ϕ is the filling factor of dust aggregates.
- (4) The compressive strength P_c is also derived from the geometrical structure as $P_c \sim (E_{\text{roll}}/r_0^3)\phi^{(2+\alpha)/(3-D_f)}$, where E_{roll} is the energy needed to rotate a monomer around its connection point by $\pi/2$ rad. Our finding suggests that the α parameter associated with the chain length plays a significant role in the compression of dust aggregates. In addition, the average coordination number Z is derived from the geometrical structure as $Z = 2 + C\phi^{D_f/(3-D_f)}$, where $C \sim 9$ is the number of the inter-cell contacts per BCCA cell.

Acknowledgment

We are grateful to Misako Tatsuuma, Akimasa Kataoka, and Hidekazu Tanaka for providing snapshots of compressed BCCA clusters and the simulation code for preparing BCCA clusters. We also thank Satoshi Okuzumi, Hiroaki Katsuragi, and Sin-iti Sirono for their fruitful discussions and comments. S.A. is supported by the Grant-in-Aid for JSPS Research Fellow (JP17J06861). This work is supported by JSPS KAKENHI grant (JP18K03721).

References

- [1] C. M. Sorensen, *Aerosol Sci. Tech.*, **35**, 648 (2001)
- [2] K. Ohno and S. Okuzumi, *Astrophys. J.*, **859**, 34 (2018)
- [3] K. Ohno, S. Okuzumi, and R. Tazaki, arXiv:1908.02201 [astro-ph.EP]
- [4] I. Adachi, C. Hayashi, and K. Nakazawa, *Prog. Theor. Phys.*, **56**, 1756 (1976)
- [5] C. Dominik and A. G. G. M. Tielens, *Astrophys. J.*, **480**, 647 (1997)
- [6] K. Wada, H. Tanaka, T. Suyama, H. Kimura, and T. Yamamoto, *Astrophys. J.*, **677**, 1296 (2008)
- [7] H. Tanaka, K. Wada, T. Suyama, and S. Okuzumi, *Prog. Theor. Phys. Suppl.*, **195**, 101 (2012)
- [8] S. Okuzumi, H. Tanaka, H. Kobayashi, and K. Wada, *Astrophys. J.*, **752**, 106 (2012)
- [9] S. Arakawa and T. Nakamoto, *Astrophys. J. Lett.*, **832**, L19 (2016)
- [10] Y. Tsukamoto, S. Okuzumi, and A. Kataoka, *Astrophys. J.*, **838**, 151 (2017)
- [11] M. Tatsuuma, S. Michikoshi, and E. Kokubo, *Astrophys. J.*, **855**, 57 (2018)
- [12] P. Meakin, *Adv. Colloid Interface Sci.*, **28**, 249 (1988)
- [13] P. Meakin, *Rev. Geophys.*, **29**, 3 (1991)
- [14] J. Blum and G. Wurm, *Annu. Rev. Astron. Astrophys.*, **46**, 21 (2008)
- [15] M. Krause, J. Blum, Y. V. Skorov, and M. Trieloff, *Icarus*, **214**, 286 (2011)
- [16] N. Sakatani, K. Ogawa, Y.-i. Iijima, M. Arakawa, R. Honda, and S. Tanaka, *AIP Adv.*, **7**, 015310 (2017)
- [17] H. Kobayashi, H. Kimura, and S. Yamamoto, *Astron. Astrophys.*, **550**, A72 (2013)

-
- [18] S. Arakawa, H. Tanaka, A. Kataoka, and T. Nakamoto, *Astron. Astrophys.*, **608**, L7 (2017)
 - [19] S. Arakawa, M. Tatsuuma, N. Sakatani, and T. Nakamoto, *Icarus*, **324**, 8 (2019)
 - [20] M. Tatsuuma, A. Kataoka, and H. Tanaka, *Astrophys. J.*, **874**, 159 (2019)
 - [21] A. Kataoka, H. Tanaka, S. Okuzumi, and K. Wada, *Astron. Astrophys.*, **554**, A4 (2013)
 - [22] G. Wurm and J. Blum, *Icarus*, **132**, 125 (1998)
 - [23] S. Kempf, S. Pfalzner, and Th. K. Henning, *Icarus*, **141**, 388 (1999)
 - [24] S. Okuzumi, H. Tanaka, and M.-a. Sakagami, *Astrophys. J.*, **707**, 1247 (2009)
 - [25] T. Mukai, H. Ishimoto, T. Kozasa, J. Blum, and J. M. Greenberg, *Astron. Astrophys.*, **262**, 315 (1992)
 - [26] R. Tazaki, H. Tanaka, S. Okuzumi, A. Kataoka, and H. Nomura, *Astrophys. J.*, **823**, 70 (2016)
 - [27] C.-h. Liu, S. R. Nagel, D. A. Schecter, S. N. Coppersmith, S. Majumdar, O. Narayan, and T. A. Witten, *Science*, **269**, 513 (1995)
 - [28] S.-i. Sirono, *Meteor. Planet. Sci.*, **49**, 109 (2014)
 - [29] T. Suyama, K. Wada, and H. Tanaka, *Astrophys. J.*, **684**, 1310 (2008)
 - [30] A. Kataoka, H. Tanaka, S. Okuzumi, and K. Wada, *Astron. Astrophys.*, **557**, L4 (2013)
 - [31] S. J. Weidenschilling, *Astrophys. Space Sci.*, **51**, 153 (1977)
 - [32] C. Hayashi, *Prog. Theor. Phys. Suppl.*, **70**, 35 (1981)
 - [33] P. Meakin, *Phys. Rev. Lett.*, **51**, 1119 (1983)
 - [34] R. Jullien and M. Kolb, *J. Phys. A*, **17**, L639 (1984)
 - [35] A. V. Luikov, A. G. Shashkov, L. L. Vasiliev, and Yu. E. Fraiman, *Int. J. Heat Mass Transfer*, **11**, 117 (1968)
 - [36] M. G. Cooper, B. B. Mikic, and M. M. Yovanovich, *Int. J. Heat Mass Transfer*, **12**, 279 (1969)
 - [37] A. Seizinger and W. Kley, *Astron. Astrophys.*, **551**, A65 (2013)
 - [38] C. Güttler, M. Krause, R. J. Geretshauser, R. Speith, and J. Blum, *Astrophys. J.*, **701**, 130 (2009)
 - [39] A. Seizinger, R. Speith, and W. Kley, *Astron. Astrophys.*, **541**, A59 (2012)
 - [40] T. Omura and A. M. Nakamura, *Planet. Space Sci.*, **149**, 14 (2017)
 - [41] T. Omura and A. M. Nakamura, *Astrophys. J.*, **860**, 123 (2018)